Nano Convergence

RESEARCH

Open Access

CrossMark

Impact of functional inorganic nanotubes f-INTs-WS$_2$ on hemolysis, platelet function and coagulation

Julie Laloy[1,2]* , Hélène Haguet[2,3] , Lutfiye Alpan[1,2], Daniel Raichman[4], Jean-Michel Dogné[1,2] and Jean-Paul Lellouche[4]*

Abstract

Inorganic transition metal dichalcogenide nanostructures are interesting for several biomedical applications such as coating for medical devices (e.g. endodontic files, catheter stents) and reinforcement of scaffolds for tissue engineering. However, their impact on human blood is unknown. A unique nanomaterial surface-engineering chemical methodology was used to fabricate functional polyacidic polyCOOH inorganic nanotubes of tungsten disulfide towards covalent binding of any desired molecule/organic species via chemical activation/reactivity of this former polyCOOH shell. The impact of these nanotubes on hemolysis, platelet aggregation and blood coagulation has been assessed using spectrophotometric measurement, light transmission aggregometry and thrombin generation assays. The functionalized nanotubes do not induce hemolysis but decrease platelet aggregation and induce coagulation through intrinsic pathway activation. The functional nanotubes were found to be more thrombogenic than the non-functional ones, suggesting lower hemocompatibility and increased thrombotic risk with functionalized tungsten disulfide nanotubes. These functionalized nanotubes should be used with caution in blood-contacting devices.

Keywords: Functional tungsten disulfide nanotubes, Safety, Hemocompatibility, Thrombin generation

1 Introduction

Inorganic transition metal dichalcogenide (TMD) materials, such as tungsten and molybdenum disulfides (WS$_2$ and MoS$_2$, respectively) are of significant interest to the scientific community because of their unique multi-layered structures and functional properties, with nano-sized fullerene-like (IF) particles tending to exhibit a different set of properties compared to the corresponding bulk forms. These metal dichalcogenide nanomaterials have emerged as one of the most promising classes of nanomaterials since the discovery of carbon nanotubes (CNTs) [1–8]. As with early researches in the field of CNTs, a wide number of potential applications have been proposed and investigated including areas such as energy storage [9], field effect transistors [10], nanocomposite coatings [11, 12], battery anodes [13], light-emitting diodes [14], self-lubricating medical devices [15], and high-performance nanoscale lubricants [16–23]. In addition, the outstanding shock absorbing ability of IFs-WS$_2$ nanotubes holds a great potential for new impact and shock-resistant materials [24–26]. Composite hybrid materials formed by incorporating small amounts (less than 5% weight ratios) of such nano-sized inorganic fillers into any given polymer matrix are also of particular interest, showing improved mechanical properties, higher thermal properties, and improved performances as barriers to heat, moisture, and solvents [27–29] when compared to similar composites prepared with conventional fillers [28, 30]. Indeed, considerable research work has been conducted dealing with polymer-based nanocomposites that incorporate inorganic IFs-WS$_2$ NPs into matrices of epoxy [30], polystyrene/poly(methylmethacrylate) [28], poly(propylene fumarate) [29], nylon 12 [31], and poly(phenylene) sulphide

*Correspondence: julie.laloy@unamur.be; lellouj@biu.ac.il
[2] Department of Pharmacy, NARILIS, University of Namur, Namur, Belgium
[4] Department of Chemistry & Institute of Nanotechnology & Advanced Materials (BINA), Bar-Ilan University, Max & Anna Web Street, 5290002 Ramat-Gan, Israel
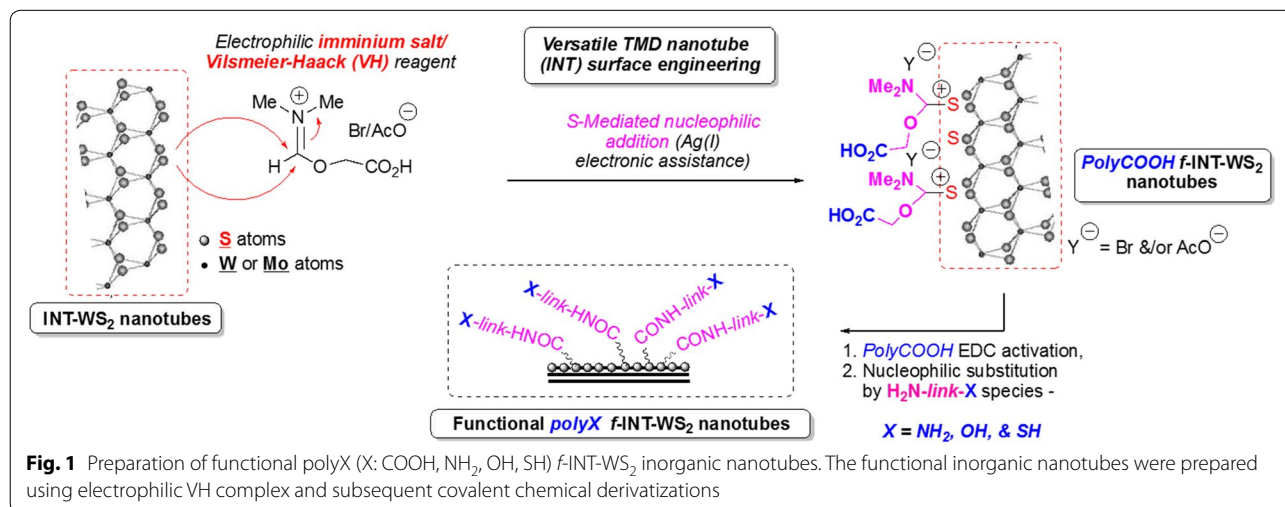Full list of author information is available at the end of the article

Springer Open

Laloy *et al. Nano Convergence*   (2018) 5:31

Page 2 of 10

[32]. Due to the superior mechanical properties of corresponding inorganic IFs-WS$_2$ NPs, such as high stiffness and strength [33], ultrahigh-performance polymer nanocomposites have been readily produced [34]. In addition, commercial performant lubricants are now presently available that include same inorganic IFs-WS$_2$ NPs that impart unique tribological properties [35] to the corresponding final composite products. Although there are many potential applications in a wide variety of fields for such inorganic metal dichalcogenide IFs-WS$_2$ NPs and inorganic INTs-WS$_2$ nanotubes (INTs), novel developmental research has been strongly hampered analogously to early CNTs-based research. Indeed, these dichalcogenide nanomaterials are highly hydrophobic, thus quite insoluble in common organic/aqueous solvents, difficult to homogeneously disperse into most liquids and resins, while disclosing serious limited dual phase compatibility when admixed with common polymers.

In this specific context, we recently developed a unique nanomaterial surface-engineering chemical methodology to fabricate covalently decorated functional polyacidic polyCOOH–INTs-WS$_2$ using Vilsmeier–Haack (VH) complex chemistry/reactivity (polyCOOH shell decoration) [36]. This novel surface engineering method enables effective covalent bonding of any desired molecule/organic species via polyCOOH shell chemical activation/reactivity that may improve and optimize any requested interfacial property of corresponding functional INTs-WS$_2$ (*f*-INTs-WS$_2$). This polycarboxylated shell can be readily exploited as an anchoring shell for subsequent second-step covalent attachment of a wide variety of organic molecules/polymers, including even other components such as NPs, for example, onto the functional nanotube surface. Therefore, a quite versatile simple organic activation chemistry (EDC•HCl activation of

polyCOOH shell/species) readily enables corresponding surface property tuning to match those requested for any contacting material (polymeric phases, solvents, etc.). Moreover and in this context, by employing appropriate bifunctional linkers such as those described in this study (obtainment of novel 2nd step polyNH$_2$/polySH/polyOH shells, Fig. 1), the resulting chemically modified *f*-INT-WS$_2$ can be covalently bound to an even wider variety of reactivity-complementing materials.

Recent progress in studies of this original novel class of inorganic nanomaterials suggests that they can be also impregnated into metallic coatings for medical administration/application [37]. For example, it was demonstrated that the use of orthodontic wires coated with metallic films containing IFs-WS$_2$ NPs in dentistry could significantly reduce the mechanical forces required for teeth realignment, thus preventing unnecessary excess forces that would lead to unacceptable teeth movement, longer treatment, and adverse damage to the roots of the teeth [10, 37, 38].

Since both IFs-WS$_2$ NPs and INTs-WS$_2$ are already commercially available in the market thus providing effective potentialities of incorporation/involvement towards innovative future medical applications, extensive research investigations concerning the overall biocompatibility and toxicity of these inorganic materials need to be performed to ensure that they are safe for composite-based usage. Researches on the toxicity of TMD nanomaterials is still in its infancy with only a handful of assessments performed on IFs-MoS$_2$ and IFs-WS$_2$ NPs. Preliminary results from in vivo toxicology tests of IFs-WS$_2$ NPs showed no apparent toxic effects on mammals, suggesting its high biocompatibility [39]. In addition, in vitro cytotoxicity examination of IFs-MoS$_2$ NPs on three different human cell lines (i.e. CCC-ESF-1,

Fig. 1 Preparation of functional polyX (X: COOH, NH$_2$, OH, SH) *f*-INT-WS$_2$ inorganic nanotubes. The functional inorganic nanotubes were prepared using electrophilic VH complex and subsequent covalent chemical derivatizations

Laloy *et al. Nano Convergence*   (2018) 5:31

Page 3 of 10

A549, and K562) revealed that they are nontoxic to cells after 48 h exposure [17]. However, at the present time, no experimental studies assessed the hemocompatibility of TMD materials. With the influx of research and possible commercialization of TMDs in the future, it is vital to both initiate hemocompatibility studies of this group of nanomaterials and assess their impact on hemolysis, platelet functions, and blood coagulation [40].

In this special work, we characterized the hemocompatibility of such different functional INTs-WS$_2$ and assessed their impact on red blood cells, platelet aggregation and blood coagulation using human blood.

2 Methods
2.1 Materials
Non-functional INTs-WS$_2$ have been bought from Nano-Materials Ltd. Company (Yavne, Israel). All reagents and solvents have been purchased from commercial sources and used without any further purification. Thermogravimetric analyses (TGA) have been performed on a TA Q600-0348, model SDT Q600 (Thermofinnigan) device using a temperature profile of 25–800 °C at 10 °C/min under nitrogen flow (180 mL/min) with sample amounts of 5–15 mg. Infrared (IR) spectra were recorded on a Fourier transform infrared spectrometer Tensor 27 (Bruker) using attenuated total reflectance (ATR). Nanomaterial surface charges were evaluated by ξ potential measurements using a Zetasizer Nano-ZS device (Malvern Instruments Ltd., United Kingdom) in water (pH adjusted) at 25 °C and 150 V. Both VH-untreated starting and resulting VH-modified f-INTs-WS$_2$ nanotubes have been also characterized using G2, FEI High Resolution transmission electron microscopy (TEM) (Tecnai). Dispersions of INT-WS$_2$ and *f*-INT-WS$_2$ have been prepared with a low-power ElmaSonic S30 bath sonicator (Elma GmbH & Co., Deutschland). The chemically accessible polyCOOH shell present on the surface of the polyCOOH *f*-INT-WS$_2$ has been also quantified by both (i) Kaiser testing after shell derivatization using 1,3-diaminopropane and (ii) Ellman's one after subsequent similar shell derivatization using cysteamine.

2.2 Polycarboxylation of INT-WS$_2$—fabrication of polyCOOH-*f*-INT-WS$_2$
To a solution of 2-bromoacetic acid (2-BrCH$_2$COOH), (1.0 g, 7.19 mmol) in anhydrous dimethyl formamide (DMF, 3 mL) was added Ag(I)OAc (10.0 mg, 0.059 mmol) and dry INT-WS$_2$ (200.0 mg). The mixture was heated in an oil bath to 80 °C and stirred over 2 days at the same temperature. After cooling to room temperature, the mixture was centrifuged (11,000 rpm, 5 min). The resulting cleaned (EtOH, 5 washing cycles) solids were dried

under vacuum to obtain 190 mg of functional polyCOOH *f*-INT-WS$_2$.

2.3 Diamine coupling onto polyCOOH *f*-INT-WS$_2$—fabrication of polyNH$_2$-*f*-INT-WS$_2$
To a solution of 1-ethyl-3-(3-dimethylaminopropyl)carbodiimide (EDC, 20.0 mg, 4 mmol) in dichloromethane (DCM, 12 mL) was added polyCOOH *f*-INT-WS$_2$ (200.0 mg) and 4-dimethylaminopyridine (DMAP, 10.0 mg, 0.08 mmol). The mixture was stirred for 2 h at room temperature followed by addition of 1,3-diaminopropane (NH$_2$–(CH$_2$)$_3$–NH$_2$, 800 µL, 9.58 mmol) and stirring continued at room temperature overnight. The mixture was centrifuged (11,000 rpm, 5 min) and the supernatant discarded. The solids were worked up as described for former polyCOOH *f*-INT-WS$_2$. The product contained 0.77 mmol NH$_2$ groups/g of polyNH$_2$ *f*-INT-WS$_2$ as determined by Kaiser testing.

2.4 Cysteamine coupling onto polyCOOH *f*-INT-WS$_2$—fabrication of polySH-*f*-INT-WS$_2$
To a solution of EDC (3.0 g, 19.32 mmol) in DCM (40 mL) was added polyCOOH *f*-INT-WS$_2$ (1.8 g). The suspension was stirred for 2 h at room temperature followed by addition of cysteamine (NH$_2$–(CH$_2$)$_2$–SH, 4.0 g, 51.85 mmol) and DMAP (20.0 mg, 0.16 mmol) and stirring continued for 2 days at room temperature. The mixture was centrifuged (11,000 rpm, 5 min) and the supernatant discarded. The solids were worked up as described for former polyCOOH *f*-INT-WS$_2$ to obtain 1.6 g of functional product. The product contained 0.8 mmol SH groups/g of polySH *f*-INT-WS$_2$, as determined by Ellman testing.

2.5 2-Aminoethanol coupling onto polyCOOH *f*-INT-WS$_2$—Fabrication of polyOH-*f*-INT-WS$_2$
To a solution of EDC (3.0 g, 19.32 mmol) in DCM (40 mL) was added polyCOOH *f*-INT-WS$_2$ (1.5 g). The suspension was stirred for 2 h at room temperature followed by addition of 2-aminoethanol (NH$_2$–(CH$_2$)$_2$–OH, 4.0 mL, 64.71 mmol) and DMAP (20.0 mg, 0.16 mmol) and stirring continued for 2 days at room temperature. The mixture was centrifuged (11,000 rpm, 5 min) and the supernatant discarded. The solids were worked up as described for former polyCOOH *f*-INT-WS$_2$ to obtain 1.3 g of functional product.

2.6 Preparation of human platelet-rich plasma, platelet-poor plasma, normal pooled plasma and washed red blood cells suspension
Human platelet rich plasma (PRP), platelet poor plasma (PPP), whole blood, washed red blood cell (RBC) suspension and normal pool plasma (NPP) were prepared with blood from healthy volunteers who were free from any

medication for at least 2 weeks. Blood was collected by venipuncture into tubes containing buffered sodium citrate (109 mM, nine parts blood to one part of sodium citrate solution) (BD Vacutainer®). The study protocol was in accordance with the Declaration of Helsinki and was approved by the Medical Ethical Committee of the CHU UCL Namur (Yvoir, Belgium).

PRP was carefully prepared by centrifugation at 200*g* of whole blood at room temperature for 10 min. The platelet count was adjusted to 300,000 platelets/µL and PRP was used immediately after preparation. Platelet free plasma used to adjust platelet concentration is obtained after centrifugation at 2000*g* in 10 min of the pellet at room temperature.

The preparation of washed RBC suspension was prepared by centrifugation of whole blood at 3000*g* over 5 min. The PPP is removed and used for interference assays. RBC are washed with physiological phosphate buffered saline (PBS, 6.7 mM phosphate, pH = 7.4) three times with intermediate centrifugation of 3000*g* over 5 min. RBC are then resuspended in PBS with the same volume as PBS removed.

For NPP, a total of 47 healthy individuals were included in the study. The exclusion criteria were thrombotic and/or hemorrhagic events, antiplatelet and/or anticoagulant medication, pregnancy and uptake of drugs potentially affecting the platelet and/or coagulation factor functions during the 2 weeks prior to the blood drawn. A written informed consent was obtained from each donor. The study population displayed the following characteristics: 27 females and 20 males aged from 18 to 53 years (mean age = 25 years) with body mass index (BMI) ranging from 17.6 to 34.9 kg/m^2 (mean BMI = 22.7 kg/m^2). After collection of blood, the PPP was obtained from the supernatant fraction of the blood tubes after a double centrifugation for 15 min at 2000*g* at room temperature. It was immediately frozen at −80 °C after centrifugation. The NPP samples were thawed and kept at 37 °C just before use.

2.7 Hemolysis assays

Hemolysis assays were performed as previously described on the blood of one healthy donor [41]. Briefly, 15 µL of nanomaterial suspended in tyrode, tyrode (negative control) or triton X-100 (positive control) are added to 285 µL of whole blood or washed RBC (final NP concentration: 100 µg/mL). The suspension is incubated at room temperature on a shaking plate during 1 h. After the incubation time, the suspension is centrifuged at 10,000*g* over 5 min. Supernatant is read in a 96-well plate using a microplate scanning spectrophotometer XMark (Biorad, USA) at 550 nm. The percentage hemolysis was then calculated as:

$$H(\%) = \frac{\left(OD_{sample} - OD_{tyrode}\right)}{\left(OD_{TritonX-100\,at\,1\%} - OD_{tyrode}\right)} \times 100.$$

For each term of the equation, the corresponding interference was subtracted. The interference corresponds to the same conditions except that the solution does not contain RBCs. Positive (triton X − 100 at 1%) and negative (Tyrode) controls induced 100% and 0% of hemolysis, respectively. The results were expressed as mean ± SD (n = 3).

2.8 Light transmission aggregometry

The impact of *f*-INTs-WS$_2$ on induced platelet aggregation was studied using the chronometric aggregometer type 490-2D as previously reported [41]. Briefly, the reaction mixture for induced aggregation tests contained 213 or 233 µL of PRP at 300,000 platelets/µL, with respectively 25 µL of collagen (final concentration: 190 µg/mL, calf skin, Bio/Data corporation, USA) or 5 µL of arachidonic acid (AA, final concentration: 600 µM, Calbiochem, Germany) and 12.5 µL of NPs at final concentration of 100 µg/mL. Inducers alone were also used before any experiment to check platelet reactivity. PPP was used as a reference. Data were collected with the chronolog two channel recorders at 405 nm connected to a computer.

2.9 Coagulation: calibrated thrombin generation test (cTGT)

The impact of non-functional and functional INTs-WS$_2$ on coagulation was studied using the calibrated thrombin generation test (cTGT) as previously reported [41]. For each experiment, a fresh mixture of fluorogenic substrate/calcium chloride buffered solution was prepared as follows: 2.6 mL of Fluo Buffer® (Thrombinoscope BV, The Netherlands) were mixed with 65 µL of Fluo substrate® (100 mM in DMSO, Thrombinoscope BV, The Netherlands). PPP-Reagent, PPP-Reagent LOW, MP-Reagent and Thrombin Calibrator (Thrombinoscope BV, The Netherlands) are four inducers, giving final assay concentrations of 5 pM tissue factor (TF) with 4 µM phospholipids (PL) and 16.7 mM CaCl$_2$; 1 pM TF with 4 µM PL and 16.7 mM CaCl$_2$; 4 µM PL and 16.7 mM CaCl$_2$; and 620 nM α2- macroglobulin-thrombin complex, respectively. They are reconstituted with 1 mL distilled water according to the instructions provided by the manufacturer. A calibration curve was simultaneously performed using the thrombin calibrator. The acquired data were automatically processed by the software, which provided thrombin activity curves and 3 parameters based on this curve: lagtime (minutes), peak concentration (nM) and endogenous thrombin potential (ETP, nM × minutes).

Laloy *et al. Nano Convergence*   (2018) 5:31

Page 5 of 10

The INT/*f*-INTs suspensions were tested at final concentrations from 5 to 500 µg/mL. Statistical analyses were conducted with an unpaired t-test using the GraphPad Prism software (GraphPad software, v 5.01, USA).

3 Results

3.1 Fabrication and characterization of *f*-INTs-WS$_2$

Functional INTs-WS$_2$ have been effectively fabricated using the two-step surface engineering methodology described in Fig. 1 below. First and as the first critical chemical modification methodology, a strongly electrophilic VH complex arising from DMF–BrCH$_2$COOH reactivity has been generated in situ in the presence of starting INTs-WS$_2$ to provide intermediate polyacidic functional polyCOOH *f*-INTs-WS$_2$.

In a 2nd derivatization step, resulting chemically modified polyCOOH *f*-INTs-WS$_2$ nanotubes might be readily chemically activated (EDC activation) and reacted with bifunctional nucleophilic linkers of the type **H$_2$N-link-X** to provide corresponding functional **polyX** (polyNH$_2$, polySH, polyOH) *f*-INTs-WS$_2$ nanotubes. All these functional nanomaterials have been fully characterized by combined thermogravimetric analysis (TGA), spectroscopic FT-IR/XPS, XRD, Kaiser (NH$_2$ species quantification)/Ellman (SH species quantification) tests, HR-TEM and ζ potential values measurements (Table 1). All these characterization spectroscopy-based spectra/data and TEM/HR-TEM microphotographs including nanomaterials are fully detailed in the corresponding Ref. [36].

3.2 Hemocompatibility

3.2.1 Red blood cells

Absorbance spectrum of RBC suspension 10% (v/v) supernatant incubated with Triton X-100 1% (v/v) is measured. The interference of nanotubes within assay is determined at 550 nm. This interference was avoided by subtracting the OD$_{550}$ nm of INTs-WS$_2$/*f*-INTs-WS$_2$ suspended in the vehicle from the measured OD$_{550}$ nm at the same concentration (data not shown). Measurement of absorbance at 550 nm in whole blood or washed RBC supernatant assesses the release of hemoglobin from lysis RBCs. Both non-functionalized and functionalized INTs-WS$_2$/*f*-INTs-WS$_2$ at 100 µg/mL did not induce hemolysis in whole blood (Fig. 2a) and in washed red blood cells (Fig. 2b) according to the ASTM E2524-08 standard (hemolysis ratio of all samples was below 5%) [42].

3.2.2 Platelet function

Second important parameter to be determined is the impact on platelet and in particular on platelet aggregation. At 100 µg/mL, non-functionalized and functionalized INTs-WS$_2$/*f*-INTs-WS$_2$ significantly decreased platelet aggregation induced by AA (Fig. 3b). When collagen is the inductor, only polyCOOH-*f*-INTs-WS$_2$ decreased significantly platelet aggregation (Fig. 3a).

3.2.3 Coagulation

Impact of *f*-INTs-WS$_2$ on blood coagulation was assessed through cTGT. Non-functionalized and functionalized INTs-WS$_2$/*f*-INTs-WS$_2$ impact blood coagulation when the intrinsic pathway is triggered (Fig. 4). A procoagulant effect of these nanomaterials is observed with a decrease of lagtime and an increase of peak concentration and ETP (Table 2). Based on their procoagulant activity on the intrinsic pathway, INTs-WS$_2$/*f*-INTs-WS$_2$ can be classified as follows: WS$_2$-NH$_2$ > WS$_2$-OH > WS$_2$-SH=WS$_2$-COOH > WS$_2$. Experiments with coagulation initiated by the extrinsic and common pathways demonstrated no effect of *f*-INTs-WS$_2$ at the exception of polyNH-*f*-INTs-WS$_2$ which had a procoagulant effect when common pathway is triggered (data not shown).
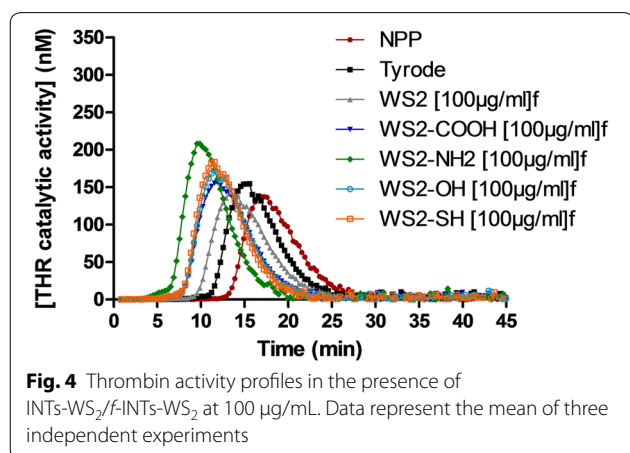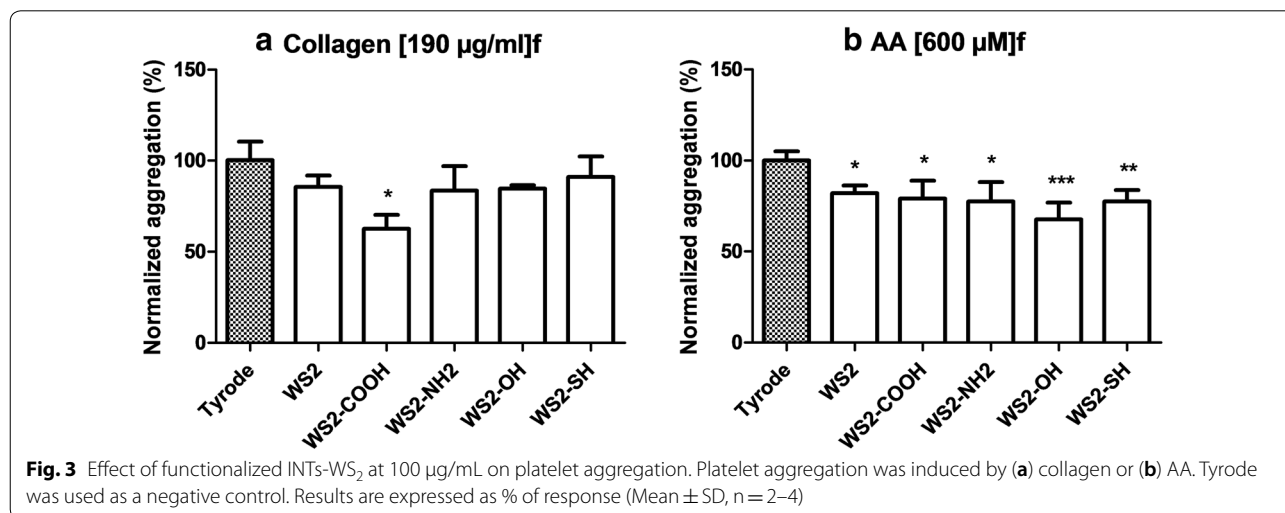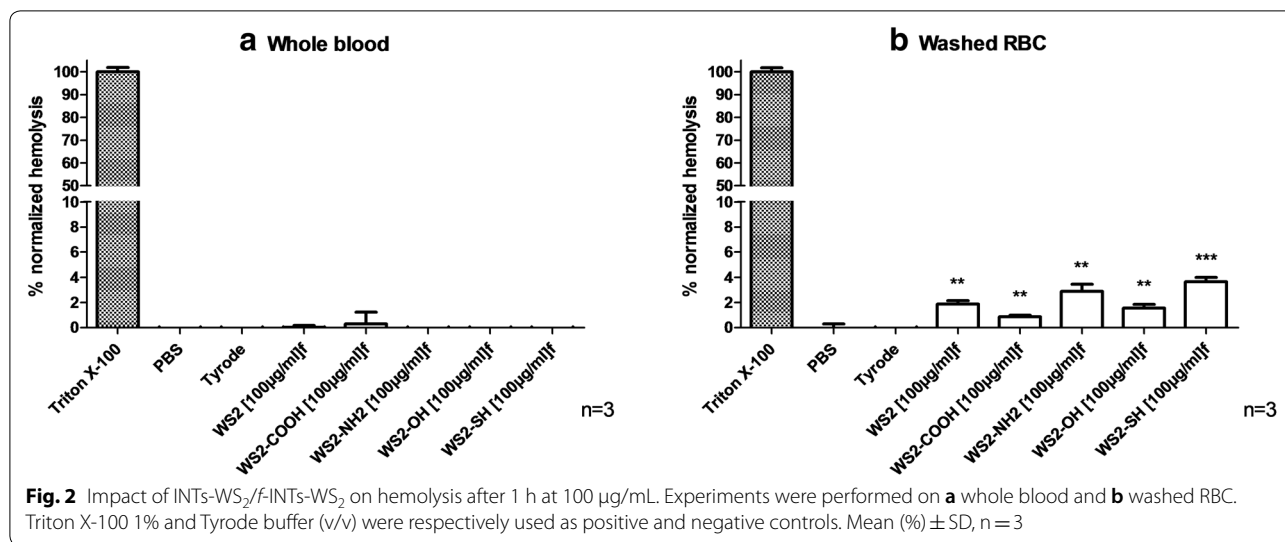
4 Discussion

As quite novel inorganic multi-layered nanomaterials, hydrophobic non-functional INTs-WS$_2$ nanotubes have been recently shown to be reactive towards a strongly

Table 1 Selected characterization (TGA) and functionality quantification data

Material	Kaiser test (mmol/g)	Ellman's test (mmol/g)	TGA—% weight loss (25–800 °C range)	ζ potential value (mV)
INTs-WS$_2$	–	–	~ 3%	− 25.0
INTs-WS$_2$COOH	–	–	11%	− 34.7
INTs-WS$_2$NH$_2$	0.77	–	19%	− 18.9
INTs-WS$_2$SH	–	0.8	14%	− 28.4
INTs-WS$_2$OH	–	–	12%	− 27.2
INTs-WS$_2$OH: specific characterizing IR data	[2683–3190–3525 cm^{-1}]: O–H stretchings set (OH organic species); 1620 and 1520 cm-1: C=O stretchings of carbonyl and amide species; 1520 cm^{-1}: C–H stretchings (saturated aliphatic species)			

INTs, inorganic nanotubes; TGA, thermogravimetric analysis—starting INTs-WS$_2$ nanotubes are negatively charged (− 25.0 mV) due to known OH-based defects arising from industrial nanofabrication step

Laloy *et al. Nano Convergence* (2018) 5:31

Page 6 of 10

Fig. 2 Impact of INTs-WS$_2$/*f*-INTs-WS$_2$ on hemolysis after 1 h at 100 µg/mL. Experiments were performed on **a** whole blood and **b** washed RBC. Triton X-100 1% and Tyrode buffer (v/v) were respectively used as positive and negative controls. Mean (%) ± SD, n = 3

Fig. 3 Effect of functionalized INTs-WS$_2$ at 100 µg/mL on platelet aggregation. Platelet aggregation was induced by (**a**) collagen or (**b**) AA. Tyrode was used as a negative control. Results are expressed as % of response (Mean ± SD, n = 2–4)

Fig. 4 Thrombin activity profiles in the presence of INTs-WS$_2$/*f*-INTs-WS$_2$ at 100 µg/mL. Data represent the mean of three independent experiments

electrophilic acidic VH complex arising from both DMF/Br-CH$_2$COOH reagents that enabled stable covalent nanotube surface chemical engineering/chemical modification by a corresponding polyCOOH shell (polyCOOH *f*-INTs-WS$_2$ nanotubes). Quite innovatively while using specific bifunctional linkers (Fig. 1), this polyacidic shell might be readily exploited via EDC activation for additional surface engineering to get a wide variety of functional *f*-INTs-WS$_2$ inorganic nanotubes, i.e., polyNH$_2$/polySH/polyOH *f*-INTs-WS$_2$ nanotubes [36]. It must be noticed that this innovative covalent surface engineering enables the quite effective development of any requested appropriate interfacial surface feature (surface reactive functionality, surface hydrophobicity/hydrophilicity

Laloy *et al. Nano Convergence*   (2018) 5:31

Page 7 of 10

Table 2 Influence of INTs-WS$_2$/*f*-INTs-WS$_2$ at 100 µg/mL on thrombin generation parameters induced by the intrinsic pathway

4 µMPL	% Lagtime	% Lagtime SD	% ETP	% ETP SD	% Peak	% Peak SD
NPP	100	9	100	9	100	11
Tyrode	81	1	110	4	112	6
WS2	71	5	107	3	102	3
WS2-COOH	58	2	114	3	113	2
WS2-NH2	48	3	130	5	150	19
WS2-OH	59	3	119	6	122	10
WS2-SH	58	2	119	1	131	6

ETP, endogenous thrombin potential; NPP, normal pool plasma

Data are expressed in percentage in comparison with control (PBS) (n = 3)

balance) when incorporated into any polymeric matrix for example.

Before being used in human, biocompatibility of blood contacting devices needs to be considered to detect potential deleterious effects. Cytotoxicity studies have been initiated with TMD nanomaterials and first results are encouraging. In vitro studies have been conducted in different cellular models and do not demonstrate WS$_2$ nanotubes induced cytotoxicity [43, 44]. Teo Chng confirmed this safety profile and demonstrates that WS$_2$ is the least toxic of TMD nanomaterials [45]. In vivo studies in murine models confirmed the safety of these particles [46, 47]. In addition to cytotoxicity studies, hemocompatibility assays are also part of preclinical assessment of any biomedical device according to ISO-10993-4. Common hemocompatibility testing includes hemolysis, platelet function, and coagulation assays. The hemocompatibility of TMD is to our knowledge currently unknown. For the first time, we are reporting here the impact of nonfunctional/functional INTs-WS$_2$/*f*-INTs-WS$_2$ on human blood. Additionally, physicochemical properties of nanomaterials (e.g. NP shape, hydrophilicity, solubility, size, chemical composition) are linked to toxic outcomes. As a matter of direct consequence, it has been quite attractive to determine, check, and eventually confirm how such versatile surface engineering functionalization shells might influence the hemocompatibility of corresponding surface-engineered INTs-WS$_2$.

Hemolysis refers to the destruction of red blood cells inducing release and buildup of toxic red blood cell content (i.e. hemoglobin), which may cause potential life-threatening conditions (e.g. hepatic and renal injuries). Because of their small size, nanomaterials bind red blood cells and could induce by this way hemolysis [48]. Therefore, assessment of hemolytic potential of all medical devices in contact with blood is required. We assessed the hemolytic potential of our nanomaterials using a spectrophotometric assay suitable to study of nanomaterials (i.e.

nanoparticle/nanotube interferences need to be ruled out) [49] and demonstrated that non-functionalized and functionalized INTs-WS$_2$/*f*-INTs-WS$_2$ do not impact hemolysis on human blood and washed red blood cells (i.e. results below the 5% threshold) in accordance to ISO-10993-4. Higher levels of hemolysis are reported in experiments with washed red blood cells compared to those performed in whole blood. This difference was previously reported with silver and silica nanoparticles and is possibly related to the adsorption of human plasma biomolecules on nanoparticles, which possibly affect their hemolytic potential [41, 50]. Our results are in accordance with prior studies, which demonstrated no hemolytic effect of other TMD nanomaterials (i.e. MoSe$_2$ nanosheets) [51, 52]. Li et al. [53] demonstrated that coating of TiNi alloy with tungsten nanomaterial reduces hemolysis rate, which confirms the safety of such materials toward red blood cells [54]. Our results are also in accordance to prior studies that indicate that nanomaterials with anionic surface does not induce hemolysis [40]. The few effect of these nanotubes on red blood cells is reassuring for future biomedical applications.

Platelet function is also part of preclinical characterization and is an important parameter to predict impact of nanomaterials on human blood clotting. Indeed, hemostasis is regulated by both plasmatic coagulation and platelet functions and alteration of platelet functions may lead to either bleeding or thrombosis [55]. Our study assessed platelet aggregation on human blood by light transmission aggregometry following activation by two different inducers, a suitable method to assess nanomaterial potential [56]. We demonstrate nonsignificant decrease of collagen-induced platelet aggregation by *f*-INTs-WS$_2$ and also that same *f*-INTs-WS$_2$ decrease platelet aggregation when induced by arachidonic acid. To our best knowledge, no other investigated impact of such nanomaterials on platelet functions has been ever reported. Therefore, the mechanism by which

Laloy *et al. Nano Convergence*   (2018) 5:31

Page 8 of 10

f-INTs-WS$_2$ induced decreased platelet aggregation is unknown. Potential hypothesis to explain this effect on platelets could be that these nanomaterials decrease agonist-induced activation. Additionally, the hydrophobicity of functional groups might be implicated in the decreased platelet aggregation. Indeed, Elbert and Hubbell have demonstrated that hydrophobic surfaces adsorb more proteins which might cause platelet adhesion and activation and therefore be responsible of blood clot [57]. This might explain why functionalization through addition of highly hydrophilic COOH groups reduces collagen-induced platelet aggregation.

As foreign materials, biomedical devices can activate human blood coagulation and dysregulate hemostasis. Human blood coagulation is characterized by a cascade of sequential proteolytic reactions which can be initiated by two pathways, the intrinsic and extrinsic ones, that both converge to thrombin generation [55]. Because coagulation is dependent to thrombin, we studied the impact of our various nanotubes on human coagulation through a thrombin generation assay, a suitable method to assess nanomaterial impact on coagulation [58] compared to routine tests, which are insensitive for small changes [55]. An additional advantage of this test is that it is performed on human plasma, a protein-containing media which limits nanomaterial interference by their coating with physiological proteins [55]. We demonstrate that non-functional INTs-WS$_2$ possess a procoagulant activity, which is accentuated by the functionalization feature of relating corresponding functional *f*-INTs-WS$_2$ nanomaterials. This procoagulant effect is mediated by activation of the intrinsic pathway while INTs-WS$_2$ do not affect the extrinsic pathway (data not shown). This is in line with data prior studies which indicate that nanomaterials mainly activate coagulation through intrinsic pathway [55].

The mechanism by which *f*-INTs-WS$_2$ induce coagulation is unknown. Numerous nanomaterial physicochemical properties are implicated in hemocompatibility and nanomaterial surface is predominant because of its interactions with plasma proteins [59]. Zeta potential is an indicator of surface charge and has been already used to predict nanomaterial effects on human health [60]. Indeed, negatively charged surfaces are expected to be more thrombogenic because contact with anionic surface initiates physiological coagulation [61]. An hypothesis suggests that the procoagulant effect of some nanomaterials is the consequence of their binding capacity with coagulation factors which induce their activation [59]. Factor XII, a factor implicated in the intrinsic pathway, is of special interest and might undergo self-activation after interaction with an anionic surface [61]. Additionally, it was already

demonstrated that anionic carbon nanotubes effectively induce human coagulation through activation of the intrinsic pathway [55]. Therefore, the anionic properties of our INTs-WS$_2$ may explain their prothrombotic activity. Additionally, functionalization of our INTs-WS$_2$ modifies surface properties and decreases zeta potential values, at the exception of NH$_2$-INTs-WS$_2$ [36]. Our study reports correlation between thrombotic potential of *f*-INTs-WS$_2$ and their zeta potential, at the exception of NH$_2$-INTs-WS$_2$. However, surface charges are difficult to interpret because of binding of proteins on nanomaterial surface and because zeta potential was determined in protein-free media (i.e. in water) compared to coagulation testing performed in human plasma. Finally, it is interesting to highlight that in our study, TGA weight loss correlates with TGTc peak concentration, with higher weight loss and procoagulant activity with NH$_2$-INTs-WS$_2$. TGA determines the amount of organic material bound to the *f*-INTs [36]. Therefore and together with their unique zwitterionic surface charge features (mixed positive ammonium/NH$_3^+$ charges with negative OH-based defects), one might speculate that NH$_2$-INTs-WS$_2$ might better promote and bind highest amounts of organic materials to more effectively induce coagulation by better binding coagulation factors.

Tungsten disulfide nanostructures possess interesting physicochemical properties and high load bearing properties implying new opportunities in medicine [47, 62]. Potential health applications include blood-contacting and invasive devices (e.g. medical device coating, drug delivery inorganic systems, reinforcement of scaffolds for tissue engineering) [32, 46]. Moreover and quite recently, same NH$_2$-INTs-WS$_2$ nanomaterials have been successfully derivatized by nanotube surface-localised C-quantum dots towards both (i) cancer cell fluorescence imaging/investigation, and (ii) quite effective photothermal cell killing capability (PTT therapy potentiality), [63] thus opening a quite attractive future field of PTT cancer therapy by such non-toxic inorganic nanotubes (nanoparticle theranostics) [64, 65]. Serious concerns exist about nanomaterial-induced coagulation disorders. Therefore, the analysis of nanomaterial toxic effects on human blood cells is quite mandatory. We demonstrated using in vitro models that INTs-WS$_2$ decrease platelet aggregation and induce a procoagulant state that is heighten by both functionalization type and level of innovative functional nanotubes. This observed effect on coagulation can be either beneficial or adverse according to its applications Therefore, we recommend the use of the functionalized nanoparticles in applications that imply blood coagulation such as wound dressing.

Abbreviations

AA: arachidonic acid; ATR: attenuated total reflectance; BMI: body mass index; CNT: carbon nanotube; cTGT: calibrated thrombin generation test; DCM: dichloromethane; DMAP: 4-dimetylaminopyridine; DMF: dimethyl formamide; EDC: 1-ethyl-3-(3-dimethylaminopropyl)carbodiimide; ETP : endogenous thrombin potential; f-INT: functional inorganic nanotube; IF: fullerene-like; IR: infrared; MbS_2: molybdenum disulfide; NPP: normal pool plasma; PL: phospholipid; PPP: platelet-poor plasma; PRP: platelet-rich plasma; RBC: red blood cell; TEM: transmission electron microscopy; TF: tissue factor; TGA: thermogravimetric analyses; TMD: transition metal dichalcogenide; VH: Vilsmeier–Haack; WS_2: tungsten disulfide.

Authors' contributions

JL and JPL designed the study. DR and JPL fabricated and characterized the nanomaterials. LA performed the hemocompatibility experiments. LA, JL and JPL analyzed and interpreted the data. JL, HH and JPL were major contributors in writing the manuscript. All authors read and approved the final manuscript.

Author details

[1] Namur Nanosafety Centre, University of Namur, Rue de Bruxelles 61, 5000 Namur, Belgium. [2] Department of Pharmacy, NARILIS, University of Namur, Namur, Belgium. [3] Department of Haematology Laboratory, Université catholique de Louvain, CHU UCL Namur, NARILIS, Yvoir, Belgium. [4] Department of Chemistry & Institute of Nanotechnology & Advanced Materials (BINA), Bar-Ilan University, Max & Anna Web Street, 5290002 Ramat-Gan, Israel.

Competing interests

The authors declare that they have no competing interests.

Availability of data and materials

The datasets used and/or analysed during the current study are available from the corresponding author on reasonable request.

Publisher's Note

Springer Nature remains neutral with regard to jurisdictional claims in published maps and institutional affiliations.

References

1. S. Bertolazzi, M. Gobbi, Y. Zhao, C. Backes, P. Samorì, Molecular chemistry approaches for tuning the properties of two-dimensional transition metal dichalcogenides. Chem. Soc. Rev. **47**(17), 6845–6888 (2018)
2. Z. Cai, B. Liu, X. Zou, H.-M. Cheng, Chemical vapor deposition growth and applications of two-dimensional materials and their heterostructures. Chem. Rev. **118**(13), 6091–6133 (2018)
3. R. Dong, I. Kuljanishvili, Review article: progress in fabrication of transition metal dichalcogenides heterostructure systems. J. Vac. Sci. Technol. **35**(3), 030803 (2017)
4. A. Eftekhari, Tungsten dichalcogenides (WS2, WSe2, and WTe2): materials chemistry and applications. J. Mater. Chem. **5**(35), 18299–18325 (2017)
5. J. Ping, Z. Fan, M. Sindoro, Y. Ying, H. Zhang, Recent advances in sensing applications of two-dimensional transition metal dichalcogenide nanosheets and their composites. Adv. Func. Mater. **27**(19), 1605817 (2017)
6. M. Samadi, N. Sarikhani, M. Zirak, H. Zhang, H.-L. Zhang, A.Z. Moshfegh, Group 6 transition metal dichalcogenide nanomaterials: synthesis, applications and future perspectives. Nanoscale Horizons. **3**(2), 90–204 (2018)
7. J. Shi, M. Hong, Z. Zhang, Q. Ji, Y. Zhang, Physical properties and potential applications of two-dimensional metallic transition metal dichalcogenides. Coord. Chem. Rev. **376**, 1–19 (2018)
8. Y. Zhou, Z. Huang, R. Yang, J. Liu, Selection and screening of DNA aptamers for inorganic nanomaterials. Chemistry **24**(11), 2525–2532 (2018)
9. M.F.L. De Volder, S.H. Tawfick, R.H. Baughman, A.J. Hart, Carbon nanotubes: present and future commercial applications. Science **339**(6119), 535–539 (2013)
10. R. Tenne, M. Redlich, Recent progress in the research of inorganic fullerene-like nanoparticles and inorganic nanotubes. Chem. Soc. Rev. **39**(5), 1423–1434 (2010)
11. H.Y. Zhao, S.T. Oyama, E.D. Naeemi, Hydrogen storage using heterocyclic compounds: the hydrogenation of 2-methylthiophene. Catal. Today **149**(1–2), 172–184 (2010)
12. B. Radisavljevic, A. Radenovic, J. Brivio, V. Giacometti, A. Kis, Single-layer MoS2 transistors. Nat. Nanotechnol. **6**(3), 147–150 (2011)
13. T. Hübert, H. Hattermann, M. Griepentrog, Sol–gel-derived nanocomposite coatings filled with inorganic fullerene-like WS2. J. Sol-Gel. Sci. Technol. **51**(3), 295–300 (2009)
14. T. Polcar, A. Nossa, M. Evaristo, A. Cavaleiro, Nanocomposite coatings of carbon-based and transition metal dichalcogenides phases—a review. Rev. Adv. Mater. Sci. **15**(2), 118–126 (2007)
15. C. Feng, L. Huang, Z. Guo, H. Liu, Synthesis of tungsten disulfide (WS2) nanoflakes for lithium ion battery application. Electrochem. Commun. **9**(1), 119–122 (2007)
16. G.L. Frey, K.J. Reynolds, R.H. Friend, H. Cohen, Y. Feldman, Solution-processed anodes from layer-structure materials for high-efficiency polymer light-emitting diodes. J. Am. Chem. Soc. **125**(19), 5998–6007 (2003)
17. A. Katz, M. Redlich, L. Rapoport, H.D. Wagner, R. Tenne, Self-lubricating coatings containing fullerene-like WS2 nanoparticles for orthodontic wires and other possible medical applications. Tribol. Lett. **21**(2), 135–139 (2006)
18. M. Ratoi, V.B. Niste, J. Walker, J. Zekonyte, Mechanism of action of WS2 lubricant nanoadditives in high-pressure contacts. Tribol. Lett. **52**(1), 81–91 (2013)
19. R. Greenberg, G. Halperin, I. Etsion, R. Tenne, The effect of WS2 nanoparticles on friction reduction in various lubrication regimes. Tribol. Lett. **17**(2), 179–186 (2004)
20. O. Eidelman, H. Friedman, R. Rosentsveig, A. Moshkovith, V. Perfiliev, S.R. Cohen et al., Chromium-rich coatings with Ws2 nanoparticles containing fullerene-like structure. Nano **06**(04), 313–324 (2011)
21. J.F. Wu, W.S. Zhai, G.F. Jie, Preparation and tribological properties of WS2 nanoparticles modified by trioctylamine. Proc. Inst. Mech. Eng. **223**(4), 695–703 (2009)
22. F. Abate, V. D'Agostino, R. Di Giuda, A. Senatore, Tribological behaviour of MoS2 and inorganic fullerene-like WS2 nanoparticles under boundary and mixed lubrication regimes. Tribology **4**(2), 91–98 (2013)
23. L. Rapoport, Y. Bilik, Y. Feldman, M. Homyonfer, Hollow nanoparticles of WS2 as potential solid-state lubricants. Nature **387**(6635), 791 (1997)
24. L. Rapoport, Y. Feldman, M. Homyonfer, H. Cohen, J. Sloan, J.L. Hutchison et al., Inorganic fullerene-like material as additives to lubricants: structure–function relationship. Wear **225**, 975–982 (1999)
25. Y.Q. Zhu, T. Sekine, K.S. Brigatti, S. Firth, R. Tenne, R. Rosentsveig et al., Shock-wave resistance of WS2 nanotubes. J. Am. Chem. Soc. **125**(5), 1329–1333 (2003)
26. Y.Q. Zhu, T. Sekine, Y.H. Li, M.W. Fay, Y.M. Zhao, C.H. Patrick Poa et al., Shock-absorbing and failure mechanisms of WS2 and MoS2 nanoparticles with fullerene-like structures under shock wave pressure. J. Am. Chem. Soc. **127**(46), 16263–16272 (2005)
27. J. Cook, S. Rhyans, L. Roncase, G. Hobson, C. Luhrs, Microstructural study of IF-WS2 failure modes. Inorganics **2**(3), 377–395 (2014)
28. M. Naffakh, A. Díez-Pascual, Thermoplastic polymer nanocomposites based on inorganic fullerene-like nanoparticles and inorganic nanotubes. Inorganics **2**(2), 291–312 (2014)

Laloy *et al. Nano Convergence*   (2018) 5:31

Page 10 of 10

29. E. Zohar, S. Baruch, M. Shneider, H. Dodiuk, S. Kenig, R. Tenne et al., The effect of WS2 nanotubes on the properties of epoxy-based nanocomposites. J. Adhes. Sci. Technol. **25**(13), 1603–1617 (2012)

30. L. Chang, H. Yang, W. Fu, N. Yang, J. Chen, M. Li et al., Synthesis and thermal stability of W/WS2 inorganic fullerene-like nanoparticles with core–shell structure. Mater. Res. Bull. **41**(7), 1242–1248 (2006)

31. W. Zhang, S. Ge, Y. Wang, M.H. Rafailovich, O. Dhez, D.A. Winesett et al., Use of functionalized WS2 nanotubes to produce new polystyrene/polymethylmethacrylate nanocomposites. Polymer **44**(7), 2109–2115 (2003)

32. G. Lalwani, A.M. Henslee, B. Farshid, P. Parmar, L. Lin, Y.X. Qin et al., Tungsten disulfide nanotubes reinforced biodegradable polymers for bone tissue engineering. Acta Biomater. **9**(9), 8365–8373 (2013)

33. F. Xu, C. Yan, Y.T. Shyng, H. Chang, Y. Xia, Y. Zhu, Ultra-toughened nylon 12 nanocomposites reinforced with IF-WS2. Nanotechnology **25**(32), 325701 (2014)

34. A. Díez-Pascual, M. Naffakh, Inorganic nanoparticle-modified poly(phenylene sulphide)/carbon fiber laminates: thermomechanical behaviour. Materials **6**(8), 3171–3193 (2013)

35. O. Tevet, O. Goldbart, S.R. Cohen, R. Rosentsveig, R. Popovitz-Biro, H.D. Wagner et al., Nanocompression of individual multilayered polyhedral nanoparticles. Nanotechnology **21**(36), 365705 (2010)

36. D. Raichman, D.A. Strawser, J.-P. Lellouche, Covalent functionalization/ polycarboxylation of tungsten disulfide inorganic nanotubes (INTs-WS2). Nano Res. **8**(5), 1454–1463 (2014)

37. Consumer products inventory 2014. http://www.nanotechproject.org/ cpi/search-products/?%20title=nanolub

38. M. Naffakh, A.M. Díez-Pascual, C. Marco, G.J. Ellis, M.A. Gómez-Fatou, Opportunities and challenges in the use of inorganic fullerene-like nanoparticles to produce advanced polymer nanocomposites. Prog. Polym. Sci. **38**(8), 1163–1231 (2013)

39. A.R. Adini, M. Redlich, R. Tenne, Medical applications of inorganic fullerene-like nanoparticles. J. Mater. Chem. **21**(39), 15121 (2011)

40. M.A. Dobrovolskaia, P. Aggarwal, J.B. Hall, S.E. McNeil, Preclinical studies to understand nanoparticle interaction with the immune system and its potential effects on nanoparticle biodistribution. Mol. Pharm. **5**(4), 487–495 (2008)

41. J. Laloy, V. Minet, L. Alpan, F. Mullier, S. Beken, O. Toussaint et al., Impact of silver nanoparticles on haemolysis, platelet function and coagulation. Nanobiomedicine **1**, 4 (2014)

42. J. Choi, V. Reipa, V.M. Hitchins, P.L. Goering, R.A. Malinauskas, Physicochemical characterization and in vitro hemolysis evaluation of silver nanoparticles. Toxicol. Sci. **123**(1), 133–143 (2011)

43. M. Pardo, T. Shuster-Meiseles, S. Levin-Zaidman, A. Rudich, Y. Rudich, Low cytotoxicity of inorganic nanotubes and fullerene-like nanostructures in human bronchial epithelial cells: relation to inflammatory gene induction and antioxidant response. Environ. Sci. Technol. **48**(6), 3457–3466 (2014)

44. I. Corazzari, F.A. Deorsola, G. Gulino, E. Aldieri, S. Bensaid, F. Turci et al., Hazard assessment of W and Mo sulphide nanomaterials for automotive use. J. Nanoparticle Res. **16**(5), 2401 (2014)

45. W.Z. Teo, E.L. Chng, Z. Sofer, M. Pumera, Cytotoxicity of exfoliated transition-metal dichalcogenides (MoS2, WS2, and WSe2) is lower than that of graphene and its analogues. Chemistry **20**(31), 9627–9632 (2014)

46. E.B. Goldman, A. Zak, R. Tenne, E. Kartvelishvily, S. Levin-Zaidman, Y. Neumann et al., Biocompatibility of tungsten disulfide inorganic nanotubes and fullerene-like nanoparticles with salivary gland cells. Tissue Eng. **21**(5–6), 1013–1023 (2015)

47. Ganzleben C, Pelsy F, Hansen SF, Corden C, Grebot B, Sobey M. Review of environmental legislation for the regulatory control of nanomaterials: final report. DG Environment of the European Commission Project Contract No 070307/2010/580540/SER/D (2011), pp. 1–244

48. T. Mocan, Hemolysis as expression of nanoparticles-induced cytotoxicity in red blood cells. Biotechnol. Mol. Biol. Nanomed. **1**(1), 7–12 (2013)

49. M.A. Dobrovolskaia, J.D. Clogston, B.W. Neun, J.B. Hall, A.K. Patri, S.E. McNeil, Method for analysis of nanoparticle hemolytic properties in vitro. Nano Lett. **8**(8), 2180–2187 (2008)

50. J. Shi, Y. Hedberg, M. Lundin, I. Odnevall Wallinder, H.L. Karlsson, L. Moller, Hemolytic properties of synthetic nano- and porous silica particles: the effect of surface properties and the protection by the plasma corona. Acta Biomater. **8**(9), 3478–3490 (2012)

51. C. Zhong, X. Zhao, L. Wang, Y. Li, Y. Zhao, Facile synthesis of biocompatible MoSe2 nanoparticles for efficient targeted photothermal therapy of human lung cancer. RSC Adv. **7**(12), 7382–7391 (2017)

52. S. Wang, K. Li, Y. Chen, H. Chen, M. Ma, J. Feng et al., Biocompatible PEGylated MoS2 nanosheets: controllable bottom-up synthesis and highly efficient photothermal regression of tumor. Biomaterials **39**, 206–217 (2015)

53. H. Li, Y. Zheng, Y.T. Pei, J.T.M. de Hosson, TiNi shape memory alloy coated with tungsten: a novel approach for biomedical applications. J. Mater. Sci. Mater. Med. **25**(5), 1249–1255 (2014)

54. A.G. Oomen, P.M. Bos, T.F. Fernandes, K. Hund-Rinke, D. Boraschi, H.J. Byrne et al., Concern-driven integrated approaches to nanomaterial testing and assessment–report of the NanoSafety Cluster Working Group 10. Nanotoxicology **8**(3), 334–348 (2014)

55. E. Frohlich, Action of Nanoparticles on Platelet Activation and Plasmatic Coagulation. Curr. Med. Chem. **23**(5), 408–430 (2016)

56. J. Laloy, F. Mullier, L. Alpan, J. Mejia, S. Lucas, B. Chatelain et al., A comparison of six major platelet functional tests to assess the impact of carbon nanomaterials on platelet function: a practical guide. Nanotoxicology **8**(2), 220–232 (2014)

57. D.L. Elbert, J.A. Hubbell, Surface treatments of polymers for biocompatibility. Annu. Rev. Mater. Sci. **26**(1), 365–394 (1996)

58. J. Laloy, S. Robert, C. Marbehant, F. Mullier, J.P. Piret et al., Validation of the calibrated thrombin generation test (cTGT) as the reference assay to evaluate the procoagulant activity of nanomaterials. Nanotoxicology **6**(2), 213–232 (2012)

59. A.N. Ilinskaya, M.A. Dobrovolskaia, Nanoparticles and the blood coagulation system. Part II: safety concerns. Nanomedicine **8**(6), 969–981 (2013)

60. Y. Zhang, M. Yang, N.G. Portney, D. Cui, G. Budak, E. Ozbay et al., Zeta potential: a surface electrical characteristic to probe the interaction of nanoparticles with normal and cancer human breast epithelial cells. Biomed. Microdevices **10**(2), 321–328 (2008)

61. M.B. Gorbet, M.V. Sefton, Biomaterial-associated thrombosis: roles of coagulation factors, complement, platelets and leukocytes. Biomaterials **25**(26), 5681–5703 (2004)

62. H. Wu, R. Yang, B. Song, Q. Han, J. Li, Y. Zhang et al., Biocompatible inorganic fullerene-like molybdenum disulfide nanoparticles produced by pulsed laser ablation in water. ACS Nano **5**(2), 1276–1281 (2011)

63. S. Nandi, S.K. Bhunia, L. Zeiri, M. Pour, I. Nachman, D. Raichman et al., Bifunctional carbon-Dot-WS2 nanorods for photothermal therapy and cell imaging. Chemistry **23**(4), 963–969 (2017)

64. J.T. Rashkow, G. Lalwani, B. Sitharaman, In vitro bioactivity of one- and two-dimensional nanoparticle-incorporated bone tissue engineering scaffolds. Tissue Eng. **24**(7–8), 641–652 (2018)

65. W. Wang, S. Liao, M. Liu, Q. Zhao, Y. Zhu, Polymer composites reinforced by nanotubes as scaffolds for tissue engineering. Int. J. Polym. Sci. **2014**, 14 (2014)